

Slack-based tunable damping leads to a trade-off between robustness and efficiency in legged locomotion

An Mo^{1,*}, Fabio Izzì^{1,2}, Emre Cemal Gönen¹, Daniel Haeufle^{2,3}, and Alexander Badri-Spröwitz^{1,4}

¹Dynamic Locomotion Group, Max Planck Institute for Intelligent Systems, Stuttgart, 70569, Germany

²Hertie Institute for Clinical Brain Research and Center for Integrative Neuroscience, University of Tübingen, Tübingen, 72076, Germany

³Institute for Modelling and Simulation of Biomechanical Systems, Computational Biophysics and Biorobotics, University of Stuttgart, Stuttgart, 70569, Germany

⁴Department of Mechanical Engineering, KU Leuven, Leuven, 3001, Belgium

*mo@is.mpg.de

ABSTRACT

Animals run robustly in diverse terrain. This locomotion robustness is puzzling because axon conduction velocity is limited to a few ten meters per second. If reflex loops deliver sensory information with significant delays, one would expect a destabilizing effect on sensorimotor control. Hence, an alternative explanation describes a hierarchical structure of low-level adaptive mechanics and high-level sensorimotor control to help mitigate the effects of transmission delays. Motivated by the concept of an adaptive mechanism triggering an immediate response, we developed a tunable physical damper system. Our mechanism combines a tendon with adjustable slackness connected to a physical damper. The slack damper allows adjustment of damping force, onset timing, effective stroke, and energy dissipation. We characterize the slack damper mechanism mounted to a legged robot controlled in open-loop mode. The robot hops vertically and planar over varying terrains and perturbations. During forward hopping, slack-based damping improves faster perturbation recovery (up to 170 %) at higher energetic cost (27 %). The tunable slack mechanism auto-engages the damper during perturbations, leading to a perturbation-trigger damping, improving robustness at minimum energetic cost. With the results from the slack damper mechanism, we propose a new functional interpretation of animals' redundant muscle tendons as tunable dampers.

Introduction

Animals run dynamically over a wide range of terrain (Fig. 1). The unevenness and changing compliance of natural terrain demand the capability for fast and dynamic adaptation to unexpected ground conditions. However, animals' neurotransmission delays slow down sensorimotor information propagation², rendering a neuronal response impossible for as much as 5 % to 40 % of the stance phase duration, depending on the animal size¹. How animals are able to produce and maintain highly dynamic movements despite delayed sensorimotor information is, therefore, a central question in neuroscience and biorobotics^{1,3-5}.

Inherent mechanical properties of muscles facilitate the rejection of unexpected perturbations⁶⁻⁹. Muscular tissue possesses nonlinear elastic and viscous-like mechanical properties, which adapt the muscle force instantly to changes in the length or contraction velocity of the muscle-tendon fibers. These mechanical properties enable the neuro-musculoskeletal system to react to external perturbations with zero delay, a capacity termed “preflex”^{10,11}.

Intrinsic elasticity and its role in legged locomotion have been studied extensively¹²⁻¹⁶. For instance, tendons, which behave like nonlinear serial springs, store and release mechanical energy during ground contact¹² and improve shock tolerance¹⁷. Inspired by this, parallel and series elastic actuators have successfully been implemented in the design of legged robots¹⁸⁻²¹, demonstrating improved robustness at low control effort. In contrast, the functional role that damping plays in legged locomotion is less studied and understood.

Damping may produce a force outcome that is adaptive to the impact velocity. This adaptive force output may enhance the effective force output during impacts²², minimize control effort²³, stabilize motion²⁴⁻²⁶ and reject unexpected disturbances^{27,28}. Nevertheless, damping is usually minimized in the design of (bio)robotic systems as it may lead to increased energy consumption. Interestingly, vertebrates seem capable of tuning the damping produced by their muscle fibers²⁹. This suggests that tunable damping may be a solution for regulating damping forces and dissipating energy depending on the terrain conditions.

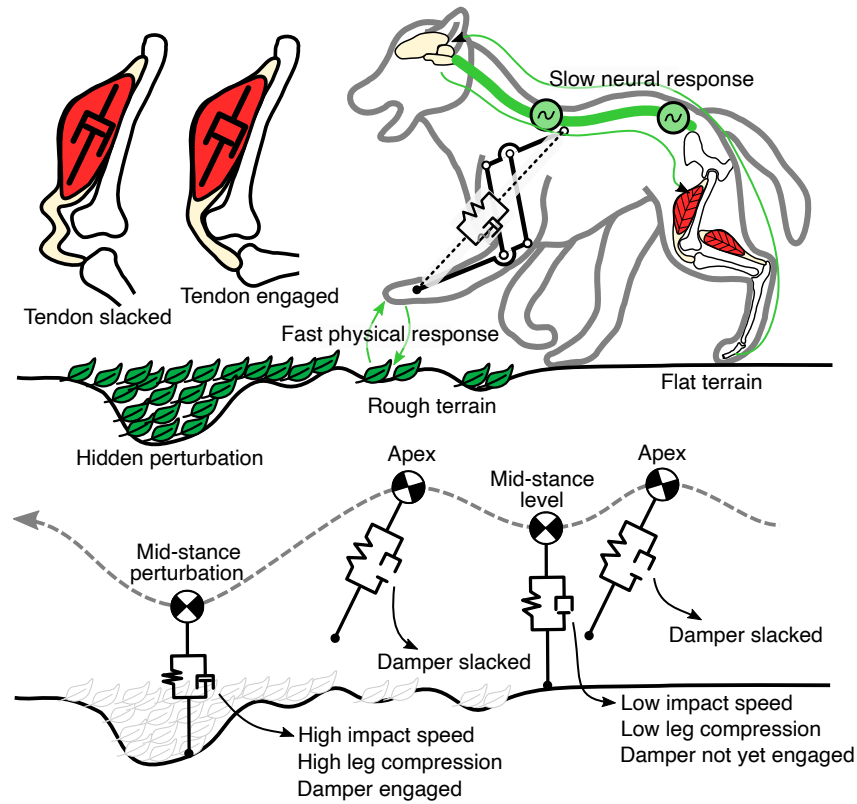


Figure 1. Top: Fast running over ground perturbation is challenging. Due to sensorimotor delays up to 50 ms, the central nervous system struggles to perceive and react to sudden ground disturbances¹. In contrast, the intrinsic mechanics of the musculoskeletal system act like a spring damper. They produce a physical and, therefore, immediate (< 5 ms) reaction when in contact with the environment. We hypothesize that the leg's damping mitigates ground disturbance through adaptive force production and energy dissipation. The tendon's slack, coupled with the joint's motion, auto-engages the damper. This creates a trade-off between locomotion robustness and energetic efficiency. **Bottom:** The damper slack enables perturbation-triggered damping. Sufficiently slacked, the damper does not engage during stance, and only spring-based torque is produced. When encountering a perturbation, the leg's compression increases further, removing all damper slack, and the damper engages in parallel to the spring.

Tunable damping in biorobotics can be implemented through control^{30,31}, i.e., virtual damping. Virtual damping poses substantial design constraints. It requires precise velocity estimation, high-frequency control (>1 kHz), strong actuators to produce sufficient peak forces, and means to dissipate the resulting heat effectively^{32–36}. Alternatively, physical dampers can be mounted to the robot's joints³⁷. Tuning damping with a physical damper mounted to a legged robot proved challenging. Setting a higher damping rate resulted in the expected higher forces, but at reduced leg compression and effective damper stroke³⁸. Consequently, the dissipated energy indicated by the work loop area did not increase. Additionally, fix-mounted physical dampers operate continuously and dissipate energy during unperturbed level running. Instead, physical tunable damping should ideally be triggered by the perturbation itself. The damper should engage and self-adjust according to the presence and severity of the ground disturbance experienced during running.

The tendon slack observed in muscle-tendon units³⁹ and animal-inspired robots⁴⁰ provided us with a design template for implementing tunable damping in a legged system (Fig. 1). By disengaging the damper from its joint via controlled tendon slack, we expect to adjust the onset, timing, and amount of damper engagement. Moreover, the tendon slack allows for a perturbation-trigger strategy (Fig. 1Bottom). During steady-state running, for example, on flat terrain, the leg compresses without saturating the tendon slack. Once an unperceived ground perturbation increases leg compression further, the tendon displacement will exceed the tendon's slack and start to auto-engage the damper. This strategy enables adaptive force output triggered by ground perturbations.

We implemented and tested a bio-inspired, physical tunable damping strategy based on tendon slack in this work. We aimed at producing perturbation-triggered damping and improving robustness against ground perturbations. We evaluated this design concept on a robotic leg during vertical and forward hopping, both in steady-state and perturbed conditions. Unlike earlier

Experiment	Terrain	Perturbation height	No. of perturbation steps	No. of repetitions
Vertical hopping	step-down	10% LL 15% LL	1	10
Forward hopping	flat terrain rough terrain rough terrain	0 mm ± 5 mm ± 10 mm	15	4
Forward hopping	ramp-up-step-down	15% LL 30% LL	1	10

Table 1. Experiment design, all experiments are repeated with damper slack values of 10, 6, 3, and 0 mm, from maximum slack to no slack.

designs³⁸, our slack damper mechanism enabled straightforward adjustment of the damper engagement and energy dissipation. We observed improved hopping robustness due to the adaptive characteristics of our physical damping design, whereas the energetic cost increases. The perturbation-triggered capacity of our slack damper mechanism allows for a more favorable trade-off between robustness and efficiency.

Results

We designed three experiments to study the proposed design with a hydraulic damper mounted to a robotic leg joint (Table 1). We tested damper slack values of 10, 6, 3, and 0 mm for all conditions. These settings span from full slack (10 mm, minimum effective damping) to no slack (0 mm, maximum effective damping). An open-loop controller produced the robot leg's locomotion pattern. Without feedback, ground perturbations were invisible to this high-level control (neural circuits), and perturbations could only be compensated by low-level mechanics in the form of a physical response.

We used the vertical hopping setup to investigate the vertical component of locomotion, allowing ground reaction force (GRF) measurement in all steps (Fig. 5d). We introduced step-down perturbation to evaluate the robustness of the system. We used the forward hopping setup, which mounts the leg on a boom structure, to simulate more realistic locomotion dynamics (Fig. 5e). We analyzed forward hopping performance on rough terrain and robustness against ramp-up-step-down perturbation.

All data can be found in Supplementary Table S3-5.

Vertical hopping with step-down perturbation

With feed-forward control, the leg hopped in the vertical setup for two perturbation levels and four slack values. Figure 2a shows an example of a time-series of 10 repetitions. The test condition included a perturbation of 15 % leg length (LL) and tendon slack of 3 mm (Supplementary Movie S1). At the perturbed step 1, the leg impacted the ground at a higher speed, compressing more. This resulted in higher damper and spring forces than during pre-perturbation levels. We noticed that the damper force did not drop to zero at midstance due to the damper's internal recovery spring.

We found that the tunable slack mechanism was effective in tuning damping. Damper slack adjustments of 0 mm to 6 mm resulted in a delayed engagement of the damper: from 0 ms to 50 ms after the onset of the spring force during level hopping (Fig. 2b). The damper's force-displacement work loops during level hopping confirmed the controllable onset of the damper force (Fig. 2c). The enclosed work loop areas represent the damper's standby dissipated energy. Damper slack values of 10, 6, 3, and 0 mm can be mapped to standby dissipation of 152, 86, 29, and 1 mJ. At the perturbation step, the damper dissipated more energy (65 % to 190 %) compared to level hopping standby dissipation (Fig. 2d). The extra dissipated energy is associated with the height of the ground drop, showing an adaptive energy dissipation to terrain disturbance. In all tested conditions, the extra dissipated energy converged to 0 in the following steps, indicating recovery to steady-state hopping.

The robustness of the hopping system can be qualitatively assessed by the phase plot of the hip height (Fig. 2e and Supplementary Movie S1). With a 10 mm slack setting, the hopping behavior was the most variable, as shown by the overlay of gray lines, representing 200 steps in 10 repetitions. With a 6 mm slack setting, the phase plot was clean, and the hopping converged to a new 'limit cycle' in fewer steps than other settings. A quantitative robustness measurement is the number of steps required to bring the system back to its original hopping height after the perturbation (Fig. 2f). The system's robustness was highest with the 6 mm slack setting, requiring on average 1.7 and 2.5 steps to recover for 10 % and 15 % LL perturbation, respectively (Fig. 2g). At stronger perturbations, the robot needed more steps to recover. We measure the energetics of the hopping system by its cost of hopping (CoH, equation (3)). The CoH increased from 6.3 to 7.6 with higher damping or stronger perturbations (Fig. 2h). With a damper slack of 6 mm at 10 % LL perturbation, we found 47 % faster perturbation recovery in combination with 5 % higher CoH compared to 10 mm damper slack (Fig. 2i).

Forward hopping with continuous perturbation

During forward hopping on the sinusoidal ground, the standard deviation of the step cycle time quantifies the hopping periodicity. In the flat terrain, the standard deviation of the step cycle time decreased from 27 ms to 2 ms with less damper slack, showing improved hopping periodicity with more damping (Fig. 3a). This tendency was less apparent in ± 5 and ± 10 mm rough terrain, as the step cycle time variation increased first for the damper slack value 6 mm, then decreased with less damper slack. The energetic cost of forward hopping was measured as the cost of transport⁴¹ (CoT, equation (4)). The CoT increased from a minimum of 0.75 to 1.35 with increasing damping (Fig. 3b). Both hopping periodicity and CoT were affected by the terrain's roughness. In flat terrain, increasing damping was associated with improved periodicity and increased CoT (Fig. 3c). At ± 5 mm terrain roughness, data for damper slack values of 0, 3, and 6 mm show similar tendency. The 10 mm damper slack shows the best performance with a CoT of 0.75 and a standard deviation of 2 ms cycle time (Fig. 3d). With ± 10 mm terrain roughness, the cycle time standard deviation was clustered around 2 mm to 3 mm for all slack settings, while the CoT varied from 0.79 to 1.32. Among these three tested terrains, the strongest damping, i.e., the setting with a slack of 0 mm, showed better periodicity with a cycle time standard deviation of ≈ 2 ms, but with the highest CoT, ranging from 1.24 to 1.35.

Forward hopping with ramp-up-step-down perturbation

We evaluated the system's robustness during forward hopping by testing its response to unexpected, sudden perturbations. Thus, we analyzed the robotic leg's behavior with step-down perturbations in its hopping path. As robustness measurement, we counted the number of steps required for the hopper to recover after the step perturbation. The second measurement of robustness is the number of failures out of ten perturbation attempts. By reducing the damper slack from 10 mm to 0 mm, the average recovery steps needed by the robotic leg decreased from 2.7 to 1.0 for the 15% LL perturbation and from 2.6 to 2.3 for the 30% LL perturbation (Fig. 4a). Similarly, with more damping, the number of failed trials decreased from 7 to 0 for the 15% LL perturbation and 10 to 3 for the 30% LL perturbation (Fig. 4b). The legged robot was less robust against a stronger perturbation, as it required on average 0.7 more recovery steps or failed, on average, four times more for the two tested perturbation levels. Similar to the other two experiments, the energetic cost of the system increased with more damping, as the CoT increased from 0.95 to 1.44 (Fig. 4c). With a damper slack of 0 mm at 15% LL perturbation, we found 170% faster perturbation recovery in combination with 27% higher CoH compared to 10 mm damper slack (Fig. 4d). With both measurements of robustness, we observed a tendency of increasing robustness at the expense of more energetic cost with higher damping settings (Fig. 4d and e).

Discussion

The slack damper mechanism allows effective tunable damping. This has three consequences: First, depending on the slack setting, the damper produces an immediate or delayed response to ground impacts (Fig. 2b). Second, the onset of the damper stroke can be reliably set by the tendon slack (Fig. 2c). Third, the mechanical work generated by the damper is tunable, as shown by the change in the size of the enclosed work loops (Fig. 2c). Such a level of tunability of the damper response was not possible in our previous, more canonical approach of controlling the damping rate of the same damper model (implemented in a two-segment leg) via orifice adjustment³⁸. In contrast, adjusting the slack of the damper tendon provides an effective strategy for tuning embedded damping in the robotic leg. The slack in the damper tendon system allows the parallel spring to soften the damper impact within tens of milliseconds after the foot touchdown. As a result, the damper produced less force and stroke than scenarios with less slack (Fig. 2c).

In the steps following a sudden drop in ground height, the additional gravitational energy results in 20% to 30% higher touchdown speeds. The damper force and negative work increase accordingly, providing a beneficial mechanical reaction to compensate for the perturbation (Fig. 2d). Therefore, our damper implementation produces mechanical work in an adaptive manner that is consistent with the perturbation level and tunable by just one parameter; the damper tendon slack.

After testing the tunability of our damper tendon system, we characterized its effect on locomotion robustness during vertical and forward hopping, with and without perturbations. In general, damping improves the robustness of our system. In the vertical hopping experiments, adding a small amount of damping (6 mm slack) led to the fastest recovery from step perturbations (Fig. 2e and g). Above a certain amount of damping, the robotic leg appears to be over-damped, as shown by the damper dissipated energy (Fig. 2d) and the hopping height over steps (Fig. 2f). In forward hopping experiments, more damping improved hopping periodicity (Fig. 3a) and robustness (Fig. 4a and b) without the emergence of an over-damping threshold. Our system performed well in this perturbed condition. It overcame the perturbation 64 times out of 80 trials, despite using the simple feed-forward open-loop controller for forward hopping motion. Although no electronic sensors are utilized to detect and respond to the perturbations, the passive compliance embedded in the leg acts as an intrinsic system of mechanical sensors and actuators, which detect and respond immediately to external disturbances. The adaptive force output from damping plays a key role. Simulation studies^{24,26} and muscle experiments⁴² have revealed the stabilizing effect of damping in legged locomotion. We offer a biorobotic understanding of damping in improving locomotion robustness.

The improved robustness introduced by the damper system comes at an energetic cost. Higher damping settings (less slack) result in higher energy costs for all the experiments (Fig. 2i, Fig. 3b, and Fig. 4c). This occurs because the actuator needs to produce more power to compensate for the lost energy by damping (Fig. 2c and d) and achieve a steady-state hopping behavior. Tunable damping leads to a trade-off between the robustness and energy cost of the system (Fig. 4d and e), despite a certain degree of nonlinearity. This trade-off implies that hopping can be either robust against perturbations but with a penalty in energy consumption, or be energy efficient but vulnerable to disturbance. Adjusting tendon slack allows for selecting a suitable compromise depending on the terrain.

The benefit of damping for legged systems remains a debate in the field^{24,43,44}. Most research on legged locomotion focuses on optimizing a single aspect, such as robustness, stability, or energy consumption. On the contrary, evolution in biology is likely not a single-objective optimization process. Instead, we argue that a more holistic perspective is required to understand the interaction among the many performance metrics characterizing legged locomotion. This study's results highlight how damping is a key to balancing the trade-off between robustness and energy consumption.

The advantage of our slack damping mechanism concerning energy consumption is that it allows a perturbation-triggered strategy. The damper tendon slack can be tuned to barely engage at level hopping. It will then engage once a ground perturbation induces higher impact velocities. In this way, the absence of a damper minimizes the dissipating energy during level hopping, while the engagement of the damper improves robustness at ground perturbation steps. This automatic on-off control was impossible with previous damper implementations^{45,46}, because damping generated from friction, rheology, eddy currents, and fluid dynamics are hard to switch off completely³⁷. Instead of optimizing the adjustment of the nonlinear damping coefficient, our mechanism features a fixed damping coefficient but exploits a slack tendon to create a tunable on-off damping. The proposed slack tendon could also be applied to selectively engage springs. Hence, the tunable tendon slack mechanism offers a new mechanism for adaptive compliant actuator applications.

Besides the adaptive force output of damping, we expect the tunability of damping to provide more optimal hopping behavior, such as transitioning into new terrain. When expecting a more uneven terrain, the damper slack can be adjusted accordingly to gain more robustness against the stronger perturbation. This requires an online slack tuning mechanism and its feedback control strategy. At the same time, we expect a feed-forward controller to be sufficient to produce highly robust running in an uncertain environment⁴⁷. Limited by the hardware implementation, we did not thoroughly investigate an online tuning design. Nevertheless, the four damper slack settings demonstrate the proof-of-concept of online tunable damping.

In summary, this work aims at understanding the tunable damping mechanism in legged locomotion. We proposed the slack damper strategy inspired by muscle tendon slack and tested it in robotic legged hopping. The slack damper mechanism allows effective tunable damping regarding onset timing, engaged stroke, and energy dissipation. This study provides novel insights into the trade-off between energetics and robustness under different damping levels. Additionally, the slack damper design allows for perturbation-trigger damping, resolving the trade-off during locomotion with unexpected perturbation. Our results could inspire future robotic locomotion hardware and controller design.

Methods

Biorobotic leg implementation

The 3-segment leg design was inspired and simplified from the leg anatomy of small mammalian quadrupeds (Fig. 5a). It consisted of four links forming a pantograph structure (Fig. 5b). A spring and a damper coupled to the knee joint mimicked the passive compliance of the quadriceps muscles. The gastrocnemius muscle and Achilles tendon were simplified as a rigid link to reduce parameter space. The two-degrees-of-freedom leg was fully actuated by two motors (hip and knee). The key design parameters are provided in the supplementary materials (Fig. S1 and Table S1).

The leg was fabricated mostly from off-the-shelf components and 3D-printing (Fig. 5c). The main structural components were 3D-printed using polylactic acid (PLA), except for the foot segment, which was 3D-printed using carbon-fiber-reinforced nylon to improve strength and impact resistance. The hip and knee motors (MN7005-KV115, *T-motor*, 1.3 Nm maximum rated torque) were placed co-axially at the hip to reduce leg swing inertia, using a 5:1 planetary gearbox (Igu35-s, *Matex*) to gear them down. The knee torque was transmitted by a timing belt (SYNCHROFLEX 10/T5/390, *Contitech*) with an additional 25:12 gear ratio. We mounted two loadcells (model 3134, *Phidgets*, 20 kg) to the spring and the damper to measure forces. The knee spring (SWS14.5-15, *MISUMI*) was designed to hold the leg in stance. Its stiffness of 10.9 N/mm was empirically determined to generate three times the body weight of the robot at 10% leg length deflection^{48,49}. The knee damper (1210M, *MISUMI*) was selected as the most effective damper from our previous study³⁸. Both the spring and the damper were coupled to the knee joint through Dyneema tendons (Climax Combat Speed 250/150, *Ockert*), with a cam radius of 30 mm and 20 mm, respectively. A roller (VMRA20-4, *MISUMI*) was attached to the piston of the damper to transform the tendon tension ("muscle lengthening") in knee flexion to a push motion on the damper piston. The whole leg weighs 0.94 kg, with a resting leg length of 31 cm.

Slack damper mechanism

Tuning an adjustable damper when operating within a legged system is challenging. Higher damping settings make the damper produce larger forces, which in turn can reduce the piston displacement, compromising the projected change in dissipated energy³⁸. Therefore, it is difficult to anticipate how adjusting the orifice of the damper internal valve affects the dissipated energy. Instead of regulating the damper's force by adjusting the orifice size, we propose damping control by adjustment of the damper tendon slack. Tendon slack has been observed in biology³⁹, as tendons can stretch up to 2 % of their nominal length before starting to produce considerable force. This is called the *toe-region* in the tendon's stress-strain diagram. Inspired by this observation, we purposely set a defined length of slack in the tendon connecting the damper to the knee joint by using the thread connection between the damper and the loadcell (Fig. 5c). The design allowed for adjusting the tendon slack by turning the screw at the end of the piston (± 1 mm per turn).

This damper slack mechanism permitted tunable damping because of two concomitant effects. First, when the ground impact flexes the leg, the parallel spring decelerates leg flexion. At the same time, the tendon slack saturates, thereby softening the engagement conditions for the damper's piston (less peak force). Second, the tendon slack reduces the damper piston stroke (less displacement). The combination of these two mechanisms—softened (less peak force) and delayed (more slack $\hat{=}$ less displacement) damper engagement—makes the integrated damper energy dissipation more predictable.

Experimental setup

We designed two experimental setups and three perturbation types to evaluate the proposed design in four slack settings.

The vertical hopping setup (Fig. 5d) investigates only the vertical component of locomotion. Such a reduced-order experiment reduced system complexity, allowing ground reaction force (GRF) measurement in all steps. The forward hopping setup (Fig. 5e) fixed the leg on a boom structure, simulating more realistic locomotion dynamics and allowing for more perturbation types.

We focus the investigation on the mechanical response produced by the passive damping embedded in the leg design. Hence, we designed an open-loop locomotion controller such that it could not detect ground perturbation. We tested three types of ground perturbations: step-down perturbation representing a sudden, unexpected disturbance during fast running; continuous perturbation simulating rough terrain conditions, and ramp-up-step-down perturbation combining gradual and sudden disturbance.

We tested damper tendon slack of 10, 6, 3, and 0 mm for each test condition. The damper engaged synchronously with the spring in the 0 mm slack setting. With the 10 mm slack setting, the damper never engaged. Hence, we investigated a wide range of possible slack conditions, from complete to zero tendon slack.

Vertical hopping

In the vertical hopping setup (Fig. 5d), the hip of the robot leg was fixed to a vertical rail (SVR-28, *MISUMI*). A force sensor (K3D60a, *ME*) was used to measure the ground reaction force during hopping. The step-down perturbation was realized using a 3D-printed block (PLA) and an automatic block-removal device. The block was placed on top of the force sensor to elevate the ground. Magnets were inserted into the block and the top plate of the force sensor to prevent relative sliding during the leg impact. The block-removal device was a lever arm actuated by a servo motor (1235M, *Power HD*). The arm pushed away the block during the aerial phase of a hopping cycle (Supplementary Movie S1). This automatic block-removal device was needed to remove the perturbation block within the aerial hopping phase reliably (200 ms in our experiments).

The vertical hopping setup was instrumented as follows. The hip position was measured by a linear encoder (AS5311, *AMS*). The loadcells (spring and damper) and the ground reaction force sensor readings were amplified (9326, *Burster*) and then recorded by a microcontroller (Due, *Arduino*) with internal 12-bit ADC. The motor position was measured by a 12-bit rotary encoder (AEAT8800-Q24, *Broadcom*). We used an open-source motor driver (Micro-Driver³⁶) for motor control, current sensing, and encoder reading, which runs dual motor field-oriented control at 10 kHz. We monitored the motor driver current with a current sensor (ACS723T-AB, *Allegro Microsystems*). A second microcontroller (Uno, *Arduino*) was implemented to control the servo motor for automatic block removal. A single-board computer (Raspberry Pi 4B) was used to centralize and synchronize all sensor readings and motor commands in 1 kHz.

We implemented a Raibert-like⁵⁰ open-loop controller for vertical hopping. The hip was position controlled with a PD controller to keep a vertical posture. The knee was torque controlled to produce a defined torque at a given duty cycle, typically during the second half of the stance phase. Motor commands are illustrated in the inserted plots in Fig. 5d. Control parameters for a stable hopping gait were found through manual tuning, resulting in a 450 ms cycle time with 100 ms knee motor push-off. The knee torque was tuned for each setting of the damper tendon slack to maintain the same hopping heights across tested conditions (Supplementary Table S2).

We tested two perturbation levels: 31 mm and 47 mm, equivalent to 10 % and 15 % of the leg length, respectively. For each hopping trial, the robot hopped for 1 min. We analyzed ten steps before and after the perturbation. Each hopping condition was repeated ten times. We recorded in total 80 trials; two perturbations \times four slack settings \times ten repetitions.

Forward hopping

In the forward hopping setup (Fig. 5e), the robot leg was mounted on a boom in a four-bar design. This mount permits only horizontal and vertical motion in the robot's sagittal plane. The length of the boom was 1.613 m, and the travel distance of a complete revolution was around 10 m. The boom design is openly available⁵¹.

The instrumentation of the forward hopping setup was similar to that of the vertical hopping setup. The force measurement and the automatic block-removal device were incompatible with the boom setup and were removed. All the other sensors remained. Horizontal and vertical motions of the rotating boom were measured by two 11-bit rotary encoders (102-V, AMS).

We generated the forward motion of the robot leg using a feed-forward central pattern generator (CPG). In most vertebrates, CPGs contribute to controlling rhythmic motion⁵², such as locomotion. We implemented a CPG controller for the hip angle trajectory θ_{hip} :

$$\theta_{hip} = A_{hip} \cos(\Phi) + O_{hip} \quad (1)$$

$$\Phi = \begin{cases} \frac{\phi}{2D} & \phi < 2\pi D_{vir} \\ \frac{\phi + 2\pi(1 - 2D_{vir})}{2(1 - D_{vir})} & \text{else} \end{cases} \quad (2)$$

where A_{hip} is the hip angle amplitude, Φ the hip angle phase, O_{hip} the hip angle offset, D_{vir} the virtual duty factor as the fraction of time when the leg moves forward, and ϕ the oscillator's linearly progressing phase. The knee motor was torque controlled to generate push-off force in the late stance, following a fixed square-wave pattern as in the vertical hopping with the same frequency as the hip CPG. The motor commands are shown in the overlay plots of Fig. 5e. For ease of comparison, the control parameters (Supplementary Table S2) remained the same for all forward-hopping experiments.

To replicate rough terrain in a controlled way, we designed 3D-print tracks with a sinusoidal profile (Fig. 5e). The circular track was built from 3D-printed blocks. These were serially connected and taped to the floor. Each block is 360 mm long, and 27 blocks fit the circumference of the hopping path. A single, shorter connection block was added (red, Fig. 5e). This connection block prevents the hopping cycle from being entrained by the terrain harmonic perturbation pattern, e.g., repeatedly stepping onto the exact position of a cycle length of the track. We tested two rough terrains, with the amplitude of the sinusoidal perturbation being 5 mm and 10 mm. In addition, we also tested hopping on flat terrain. For each trial, the robot performed a total of six revolutions. We cropped the first and the last revolution from the recorded data and analyzed the remaining four revolutions (60 steps per condition).

Further, we designed ramp-up-step-down perturbations to disturb stable hopping during forward locomotion. Within a revolution's 10 m hopping path, we built a slope of 3 m length for the robot leg to gradually climb and jump off. We tested two perturbation heights: 47 mm and 93 mm, equivalent to 15% and 30% of leg length, respectively. For each trial, the robot leg performed 12 revolutions. We cropped the first and the last revolution from the recorded data and analyzed the remaining ten revolutions (150 steps per condition).

Data analysis

The ground reaction force and vertical position data were filtered for the vertical hopping experiments with a 4th-order zero-lag Butterworth filter. The loadcells were calibrated to output force reading only at leg flexion. The spring and damper force data were smoothed using a moving average filter with a filter span of 5 samples. The boom encoder data were filtered with a 4th-order zero-lag Butterworth filter for the forward hopping experiments. The cutoff frequencies (9 Hz-19 Hz) of the Butterworth filter were determined by residual analysis⁵³.

The recovery steps in the vertical hopping experiment were calculated by first computing the average hop height before perturbation as a reference height (dotted lines in Fig. 2f) and then finding the post-perturbation hop height that intersected with the $\pm 4\%$ boundary of the reference height²¹. The cost of hopping was calculated by normalizing the electric energy consumption E_{elec} of one hopping step to the system's gravitational potential energy at the apex.

$$CoH = \frac{E_{elec}}{m \cdot g \cdot h_{apex}} \quad (3)$$

where m is the robot mass, g the gravitational acceleration, h_{apex} the apex height position.

We defined two measurements for evaluating the robustness of forward hopping after the ramp-up-step-down perturbation. The recovery steps were defined as the number of steps needed by the robot leg to recover its stable hopping after the step-down perturbation. This metric quantified how fast the robot system can recover from perturbation, and it was measured by visual inspection of the video recordings and kinematic data. The failure step metric quantified the number of failures after a

perturbation was applied. We identified two failure modes from the video recordings: the robot leg could slip or stop after the perturbation (Supplementary Movie S3). The number of failures was visually counted from the video recordings. The CoT was calculated by the electric energy consumption per distance traveled d , normalized by the robot weight.

$$CoT = \frac{E_{elec}}{m \cdot g \cdot d} \quad (4)$$

All data were processed with Matlab (R2021b, *MathWorks*).

Data availability

All data needed to evaluate the conclusions of the paper are available in the paper or the Supplementary Information. Data and scripts for data analysis and the computer-aided design model of the robot leg are available from <https://keeper.mpdl.mpg.de/d/8fee69fa1fe7466b93bc/>.

References

1. More, H. L. *et al.* Scaling of Sensorimotor Control in Terrestrial Mammals. *Proc. Royal Soc. B: Biol. Sci.* **277**, 3563–3568, DOI: [10.1098/rspb.2010.0898](https://doi.org/10.1098/rspb.2010.0898) (2010).
2. Gordon, J. C., Holt, N. C., Biewener, A. & Daley, M. A. Tuning of feedforward control enables stable muscle force-length dynamics after loss of autogenic proprioceptive feedback. *eLife* **9**, e53908, DOI: [10.7554/eLife.53908](https://doi.org/10.7554/eLife.53908) (2020).
3. More, H. L. & Donelan, J. M. Scaling of sensorimotor delays in terrestrial mammals. *Proc. R. Soc. B* **285**, 20180613, DOI: [10.1098/rspb.2018.0613](https://doi.org/10.1098/rspb.2018.0613) (2018).
4. Kamska, V., Daley, M. & Badri-Spröwitz, A. 3D Anatomy of the Quail Lumbosacral Spinal Canal—Implications for Putative Mechanosensory Function. *Integr. Org. Biol.* **2**, DOI: [10.1093/iob/obaa037](https://doi.org/10.1093/iob/obaa037) (2020).
5. Ashtiani, M. S., Aghamaleki Sarvestani, A. & Badri-Spröwitz, A. Hybrid parallel compliance allows robots to operate with sensorimotor delays and low control frequencies. *Front. Robotics AI* **170**, DOI: [10.3389/frobt.2021.645748](https://doi.org/10.3389/frobt.2021.645748) (2021).
6. Loeb, G. E., Brown, I. E. & Cheng, E. J. A hierarchical foundation for models of sensorimotor control. *Exp. Brain Res.* **126**, 1–18, DOI: [10.1007/s002210050712](https://doi.org/10.1007/s002210050712) (1999).
7. Wagner, H. & Blickhan, R. Stabilizing function of skeletal muscles: an analytical investigation. *J. Theor. Biol.* **199**, 163–179, DOI: [10.1006/jtbi.1999.0949](https://doi.org/10.1006/jtbi.1999.0949) (1999).
8. Grillner, S. The role of muscle stiffness in meeting the changing postural and locomotor requirements for force development by the ankle extensors. *Acta Physiol. Scand.* **86**, 92–108, DOI: [10.1111/j.1748-1716.1972.tb00227.x](https://doi.org/10.1111/j.1748-1716.1972.tb00227.x) (1972).
9. Daley, M. A., Voloshina, A. & Biewener, A. A. The role of intrinsic muscle mechanics in the neuromuscular control of stable running in the guinea fowl. *The J. Physiol.* **587**, 2693–2707, DOI: [10.1113/jphysiol.2009.171017](https://doi.org/10.1113/jphysiol.2009.171017) (2009).
10. Brown, I. E., Scott, S. H. & Loeb, G. E. Preflexes—programmable high-gain zero-delay intrinsic responses of perturbed musculoskeletal systems. *Soc. Neurosci. Abstr.* **21**, 562 (1995).
11. Brown, I. E. & Loeb, G. E. A reductionist approach to creating and using neuromusculoskeletal models. In *Biomechanics and neural control of posture and movement*, 148–163, DOI: [10.1007/978-1-4612-2104-3_10](https://doi.org/10.1007/978-1-4612-2104-3_10) (Springer, 2000).
12. Alexander, R., Maloiy, G., Ker, R., Jayes, A. & Warui, C. The role of tendon elasticity in the locomotion of the camel (*Camelus dromedarius*). *J. Zool.* **198**, 293–313, DOI: [10.1111/j.1469-7998.1982.tb02077.x](https://doi.org/10.1111/j.1469-7998.1982.tb02077.x) (1982).
13. Alexander, R. M. Energy-saving mechanisms in walking and running. *The J. Exp. Biol.* **160**, 55–69, DOI: [10.1242/jeb.160.1.55](https://doi.org/10.1242/jeb.160.1.55) (1991).
14. Hof, A. L. Effects of Muscle Elasticity in Walking and Running. In *Multiple Muscle Systems*, 591–607, DOI: [10.1007/978-1-4613-9030-5_38](https://doi.org/10.1007/978-1-4613-9030-5_38) (Springer New York, New York, NY, 1990).
15. Biewener, A. A. & Roberts, T. J. Muscle and tendon contributions to force, work, and elastic energy savings: a comparative perspective. *Exerc. sport sciences reviews* **28**, 99–107 (2000).
16. Robertson, B. D. & Sawicki, G. S. Exploiting elasticity: Modeling the influence of neural control on mechanics and energetics of ankle muscle-tendons during human hopping. *J. Theor. Biol.* **353**, 121–132, DOI: [10.1016/j.jtbi.2014.03.010](https://doi.org/10.1016/j.jtbi.2014.03.010) (2014).
17. Roberts, T. J. & Azizi, E. The series-elastic shock absorber: tendons attenuate muscle power during eccentric actions. *J. applied physiology (Bethesda, Md. : 1985)* **109**, 396–404, DOI: [10.1152/jappphysiol.01272.2009](https://doi.org/10.1152/jappphysiol.01272.2009) (2010).

18. Spröwitz, A. *et al.* Towards dynamic trot gait locomotion: Design, control, and experiments with cheetah-cub, a compliant quadruped robot. *The Int. J. Robotics Res.* **32**, 932–950, DOI: [10.1177/0278364913489205](https://doi.org/10.1177/0278364913489205) (2013).
19. Grizzle, J., Hurst, J., Morris, B., Park, H.-W. & Sreenath, K. MABEL, a new robotic bipedal walker and runner. In *2009 American Control Conference*, 2030–2036, DOI: [10.1109/ACC.2009.5160550](https://doi.org/10.1109/ACC.2009.5160550) (IEEE, 2009).
20. Hubicki, C. *et al.* Atrias: Design and validation of a tether-free 3d-capable spring-mass bipedal robot. *The Int. J. Robotics Res.* **35**, 1497–1521, DOI: [10.1177/0278364916648388](https://doi.org/10.1177/0278364916648388) (2016).
21. Zhao, G., Mohseni, O., Murcia, M., Seyfarth, A. & Sharbafi, M. A. Exploring the effects of serial and parallel elasticity on a hopping robot. *Front. Neurorobotics* DOI: <https://doi.org/10.3389/fnbot.2022.919830> (2022).
22. Müller, R., Tschiesche, K. & Blickhan, R. Kinetic and kinematic adjustments during perturbed walking across visible and camouflaged drops in ground level. *J. Biomech.* **47**, 2286–2291, DOI: [10.1016/j.jbiomech.2014.04.041](https://doi.org/10.1016/j.jbiomech.2014.04.041) (2014).
23. Haeufle, D. F. B., Günther, M., Wunner, G. & Schmitt, S. Quantifying control effort of biological and technical movements: An information-entropy-based approach. *Phys. Rev. E* **89**, 012716, DOI: [10.1103/PhysRevE.89.012716](https://doi.org/10.1103/PhysRevE.89.012716) (2014).
24. Shen, Z. & Seipel, J. A fundamental mechanism of legged locomotion with hip torque and leg damping. *Bioinspiration & biomimetics* **7**, 046010, DOI: [10.1088/1748-3182/7/4/046010](https://doi.org/10.1088/1748-3182/7/4/046010) (2012).
25. Secer, G. & Saranlı, U. Control of monopedal running through tunable damping. In *2013 21st Signal Processing and Communications Applications Conference (SIU)*, 1–4, DOI: [10.1109/SIU.2013.6531557](https://doi.org/10.1109/SIU.2013.6531557) (IEEE, 2013).
26. Abraham, I., Shen, Z. & Seipel, J. A Nonlinear Leg Damping Model for the Prediction of Running Forces and Stability. *J. Comput. Nonlinear Dyn.* **10**, DOI: [10.1115/1.4028751](https://doi.org/10.1115/1.4028751) (2015).
27. Haeufle, D. F. B., Grimmer, S. & Seyfarth, A. The role of intrinsic muscle properties for stable hopping - stability is achieved by the force-velocity relation. *Bioinspiration & Biomimetics* **5**, 016004, DOI: [10.1088/1748-3182/5/1/016004](https://doi.org/10.1088/1748-3182/5/1/016004) (2010).
28. Kalveram, K. T., Haeufle, D. F. B., Seyfarth, A. & Grimmer, S. Energy management that generates terrain following versus apex-preserving hopping in man and machine. *Biol. Cybern.* **106**, 1–13, DOI: [10.1007/s00422-012-0476-8](https://doi.org/10.1007/s00422-012-0476-8) (2012).
29. Günther, M. & Schmitt, S. A macroscopic ansatz to deduce the Hill relation. *J. theoretical biology* **263**, 407–18, DOI: [10.1016/j.jtbi.2009.12.027](https://doi.org/10.1016/j.jtbi.2009.12.027) (2010).
30. Monteleone, S., Negrello, F., Catalano, M. G., Garabini, M. & Grioli, G. Damping in compliant actuation: A review. *IEEE Robotics & Autom. Mag.* **29**, 47–66, DOI: [10.1109/MRA.2021.3138388](https://doi.org/10.1109/MRA.2021.3138388) (2022).
31. Candan, S. Ş., Karagöz, O. K., Yazıcıoğlu, Y. & Saranlı, U. Design of a parallel elastic hopper with a wrapping cam mechanism and template based virtually tunable damping control. In *Dynamic Systems and Control Conference*, vol. 84270, V001T05A009, DOI: [10.1115/DSCC2020-3278](https://doi.org/10.1115/DSCC2020-3278) (American Society of Mechanical Engineers, 2020).
32. Seok, S. *et al.* Design principles for energy-efficient legged locomotion and implementation on the mit cheetah robot. *IEEE/ASME Transactions on Mechatronics* **20**, 1117–1129, DOI: [10.1109/TMECH.2014.2339013](https://doi.org/10.1109/TMECH.2014.2339013) (2015).
33. Hutter, M. *et al.* Starleth: A compliant quadrupedal robot for fast, efficient, and versatile locomotion. In *Adaptive Mobile Robotics*, 483–490, DOI: [10.1142/9789814415958_0062](https://doi.org/10.1142/9789814415958_0062) (World Scientific, 2012).
34. Havoutis, I., Semini, C., Buchli, J. & Caldwell, D. G. Quadrupedal trotting with active compliance. In *Mechatronics (ICM), 2013 IEEE International Conference on*, 610–616, DOI: [10.1109/ICMECH.2013.6519112](https://doi.org/10.1109/ICMECH.2013.6519112) (IEEE, 2013).
35. Kalouche, S. Goat: A legged robot with 3d agility and virtual compliance. In *2017 IEEE/RSJ International Conference on Intelligent Robots and Systems (IROS)*, 4110–4117, DOI: [10.1109/IROS.2017.8206269](https://doi.org/10.1109/IROS.2017.8206269) (2017).
36. Grimminger, F. *et al.* An Open Force-Controlled Modular Robot Architecture for Legged Locomotion Research. *The IEEE Robotics Autom. Lett.* DOI: [10.1109/LRA.2020.2976639](https://doi.org/10.1109/LRA.2020.2976639) (2020).
37. Vanderborght, B. *et al.* Variable impedance actuators: A review. *Robotics autonomous systems* **61**, 1601–1614, DOI: [10.1016/j.robot.2013.06.009](https://doi.org/10.1016/j.robot.2013.06.009) (2013).
38. Mo, A., Izzi, F., Haeufle, D. F. & Badri-Spröwitz, A. Effective viscous damping enables morphological computation in legged locomotion. *Front. Robotics AI* **7**, 110, DOI: [10.3389/frobt.2020.00110](https://doi.org/10.3389/frobt.2020.00110) (2020).
39. Robi, K., Jakob, N., Matevz, K. & Matjaz, V. The physiology of sports injuries and repair processes. *Curr. issues sports exercise medicine* 43–86, DOI: [10.5772/54234](https://doi.org/10.5772/54234) (2013).
40. Badri-Spröwitz, A., Aghamaleki Sarvestani, A., Sitti, M. & Daley, M. A. Birdbot achieves energy-efficient gait with minimal control using avian-inspired leg clutching. *Sci. Robotics* **7**, eabg4055, DOI: [10.1126/scirobotics.abg4055](https://doi.org/10.1126/scirobotics.abg4055) (2022).

41. Tucker, V. A. The energetic cost of moving about: walking and running are extremely inefficient forms of locomotion. much greater efficiency is achieved by birds, fish—and bicyclists. *Am. Sci.* **63**, 413–419 (1975).
42. Wilson, A. M., McGuigan, M. P., Su, A. & Van den Bogert, A. J. Horses damp the spring in their step. *Nature* **414**, 895–899 (2001).
43. Cham, J. G. & Cutkosky, M. R. Dynamic Stability of Open-Loop Hopping. *J. Dyn. Syst. Meas. Control.* **129**, 275–284, DOI: [10.1115/1.2718237](https://doi.org/10.1115/1.2718237) (2006).
44. Heim, S., Millard, M., Le Mouel, C. & Badri-Spröwitz, A. A little damping goes a long way: a simulation study of how damping influences task-level stability in running. *Biol. Lett.* **16**, 20200467, DOI: [10.1098/rsbl.2020.0467](https://doi.org/10.1098/rsbl.2020.0467) (2020).
45. Garcia, E., Arevalo, J. C., Munoz, G. & Gonzalez-de Santos, P. Combining series elastic actuation and magneto-rheological damping for the control of agile locomotion. *Robotics Auton. Syst.* **59**, 827–839, DOI: [10.1016/j.robot.2011.06.006](https://doi.org/10.1016/j.robot.2011.06.006) (2011).
46. Arelekatti, V. N. M., Petelina, N. T., Johnson, W. B., Major, M. J. & Winter V, A. G. Design of a Four-Bar Latch Mechanism and a Shear-Based Rotary Viscous Damper for Single-Axis Prosthetic Knees. *J. Mech. Robotics* **14**, DOI: [10.1115/1.4052804](https://doi.org/10.1115/1.4052804) (2021).
47. Wu, A. & Geyer, H. The 3-d spring–mass model reveals a time-based deadbeat control for highly robust running and steering in uncertain environments. *IEEE Transactions on Robotics* **29**, 1114–1124, DOI: [10.1109/TRO.2013.2263718](https://doi.org/10.1109/TRO.2013.2263718) (2013).
48. Bobbert, M. F., Yeadon, M. R. & Nigg, B. M. Mechanical analysis of the landing phase in heel-toe running. *J. Biomech.* **25**, 223–234, DOI: [10.1016/0021-9290\(92\)90022-S](https://doi.org/10.1016/0021-9290(92)90022-S) (1992).
49. Walter, R. M. & Carrier, D. R. Ground forces applied by galloping dogs. *J. Exp. Biol.* **210**, 208–216, DOI: [10.1242/jeb.02645](https://doi.org/10.1242/jeb.02645) (2007).
50. Raibert, M. *Legged Robots that Balance*. Artificial Intelligence Series (MIT Press, 1986).
51. Ruppert, F., Aghamaleki Sarvestani, A., Heim, S., Mo, A. & Badri-Spröwitz, A. Instrumented boom, CAD data, DOI: [10.17617/3.RSO2AG](https://doi.org/10.17617/3.RSO2AG) (2022).
52. Ijspeert, A. J., Crespi, A., Ryczko, D. & Cabelguen, J.-M. From swimming to walking with a salamander robot driven by a spinal cord model. *Science* **315**, 1416–1420, DOI: [10.1126/science.1138353](https://doi.org/10.1126/science.1138353) (2007).
53. Winter, D. *Biomechanics and Motor Control of Human Movement* (Wiley, 2009).

Acknowledgements

The authors thank the International Max Planck Research School for Intelligent Systems (IMPRS-IS) for supporting An Mo, Fabio Izzi, Emre Cemal Gönen, and the China Scholarship Council (CSC) for supporting An Mo. The authors thank Felix Ruppert and Alborz Aghamaleki Sarvestani for assisting the robot development. The authors also thank Prof. Syn Schmitt and Prof. Martin Giese for inspiring discussions on the project.

Author contributions

A.M., F.I., D.H., and A.B.-S. conceptualized the project, A.M., D.H., and A.B.-S. conceived the experiments A.M. designed and implemented the robot and experimental setups, A.M. and E.C.G. conducted experiments and analyzed the data, all authors interpreted and discussed the data, A.M., F.I. and E.C.G. prepared the manuscript, all authors reviewed the manuscript.

Funding

This work was funded by the Deutsche Forschungsgemeinschaft (DFG, German Research Foundation) - 449912641, HA 7170/3.

Additional information

Competing interests The authors declare no competing interests.

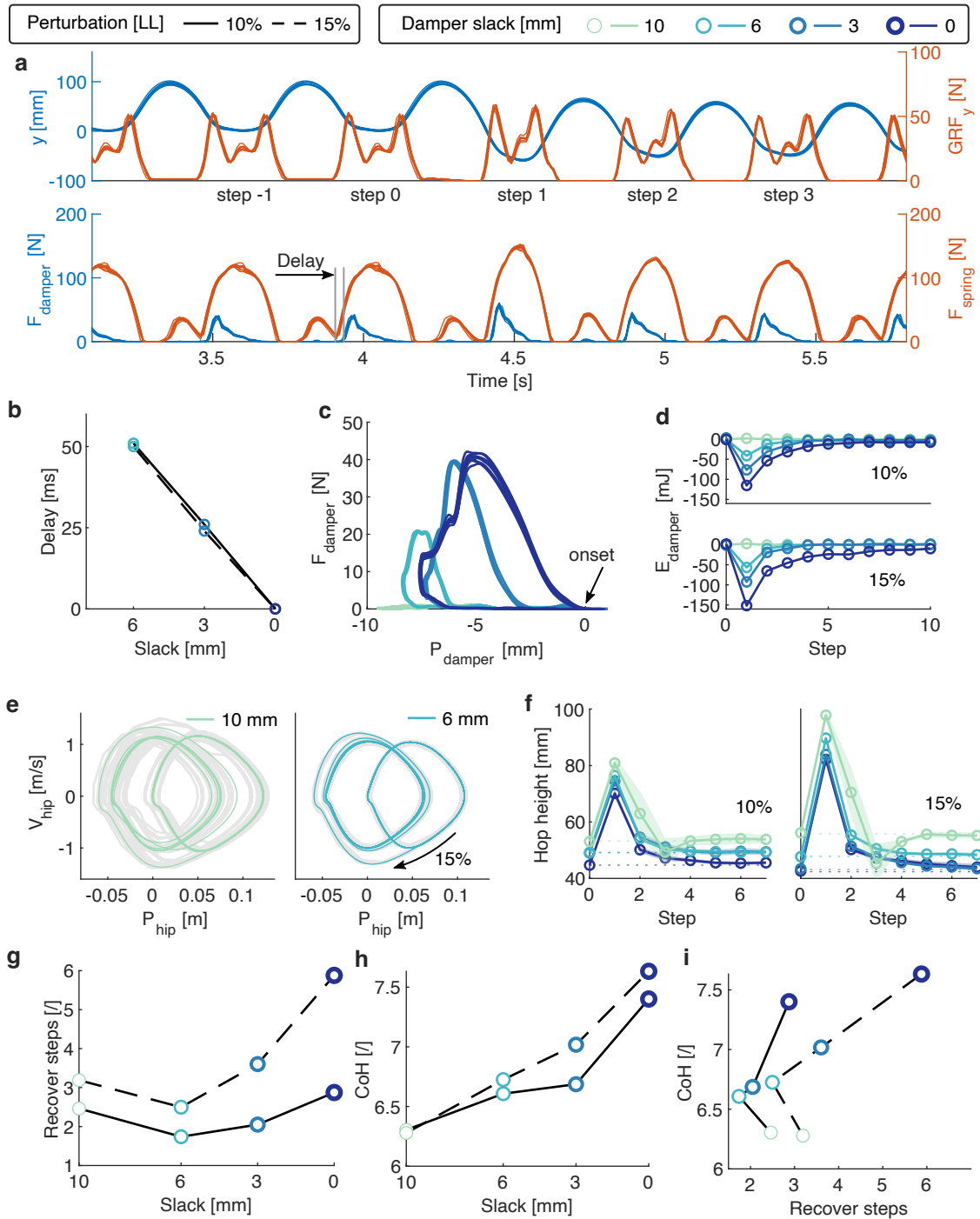


Figure 2. Vertical hopping with step-down perturbation: (a) 10-repetition-overlay time-series of hip position y , GRF, spring, and damper forces. 15% LL perturbation at step 1 increases the GRF, spring and damper forces due to higher impact speed. The damper starts to produce force with a delay to touchdown due to the 3 mm slack setting. (b) This damper engagement delay is adjustable by the damper slack setting. (c) The 10-repetition-overlay damper work loop in unperturbed periodic steps shows that the onset position can be reliably tuned and the standby dissipated energy (enclosed area) adjustable. (d) The average extra damper dissipated energy during perturbation steps. (e) Phase plot of hip position with 10 mm and 6 mm damper slack under 15% LL perturbation. The grey overlay shows the overlap of 10 repetitions of 20 steps, while the darker line is the averaged trajectory. (f) The average hopping apex height during perturbation steps. The transparent overlay represents the 95% confidence boundary. (g) The relationship between the number of steps to recovery after perturbation and the damper slack settings. (h) The relationship between the cost of hopping and the damper slack settings. (i) The relationship between the number of steps to recovery to the cost of hopping under different damper slack settings and perturbation levels.

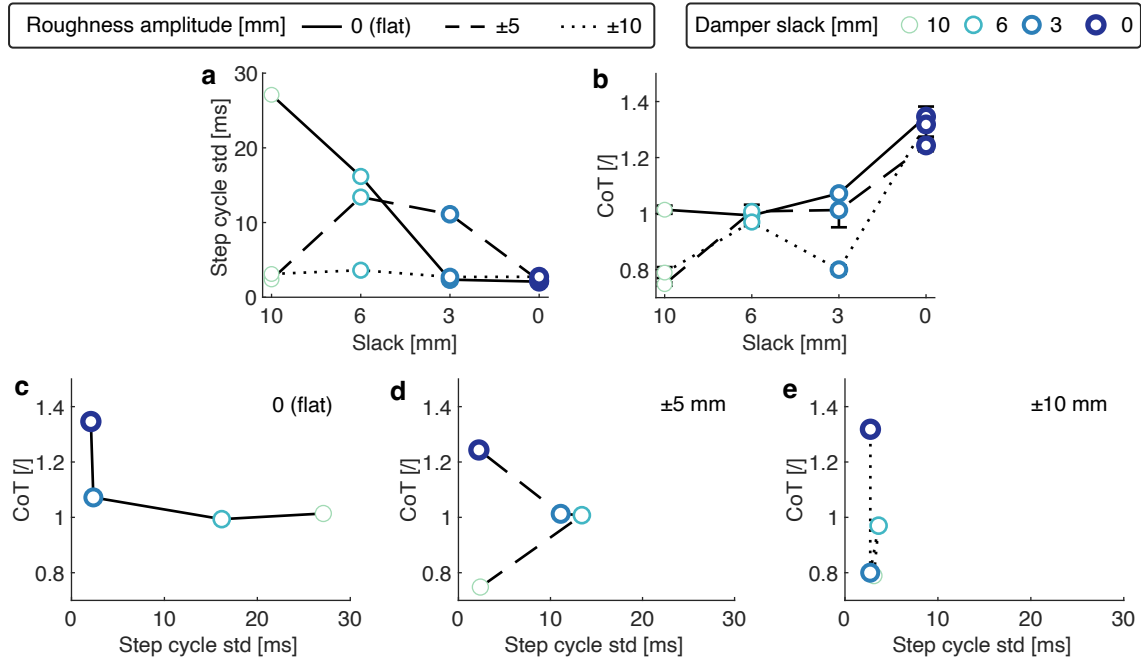


Figure 3. Forward hopping with continuous perturbation: (a) The standard deviation of the step cycle time shows that the hopping periodicity is improved with higher damping (less slack). (b) The relationship between the CoT and the damper slack settings. (c) In flat terrain, the robot's ability to maintain periodic hopping is improved by higher damping at the cost of CoT. (d, e) In the continuous perturbation terrain, high damping is also associated with high CoT and good periodicity.

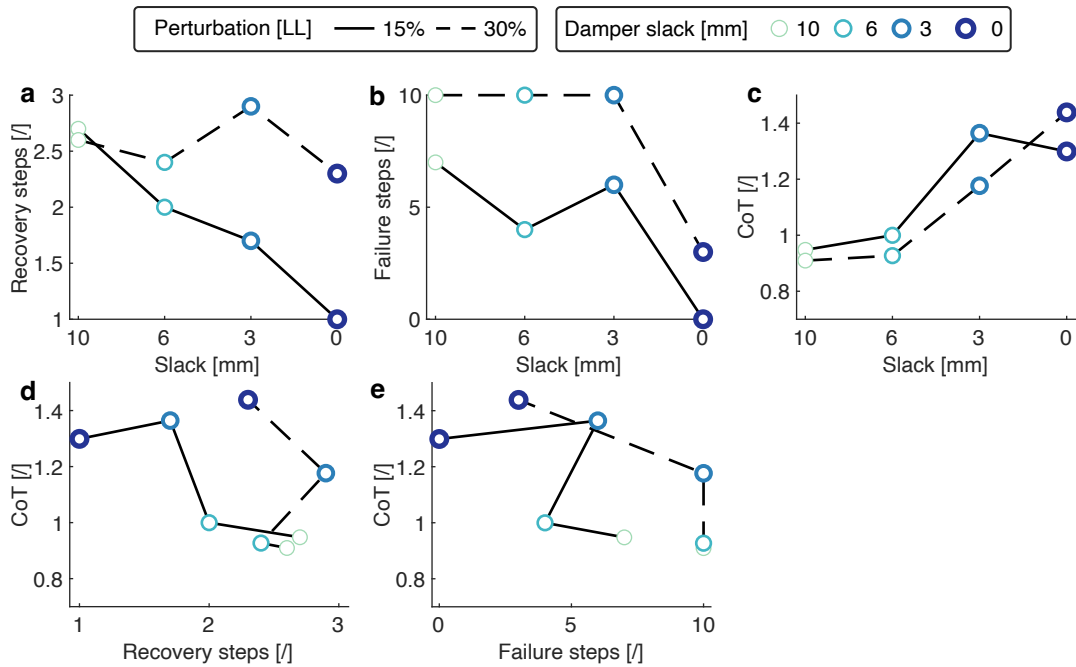


Figure 4. Forward hopping with ramp-up and step-down perturbation: The robustness of the robot system is quantified with the number of steps needed to recover stable hopping (a) and the number of failed trials in 10 attempts (b). (c) The relationship between the CoT and the damper slack settings. (d and e) show the trade-off between robustness and CoT.

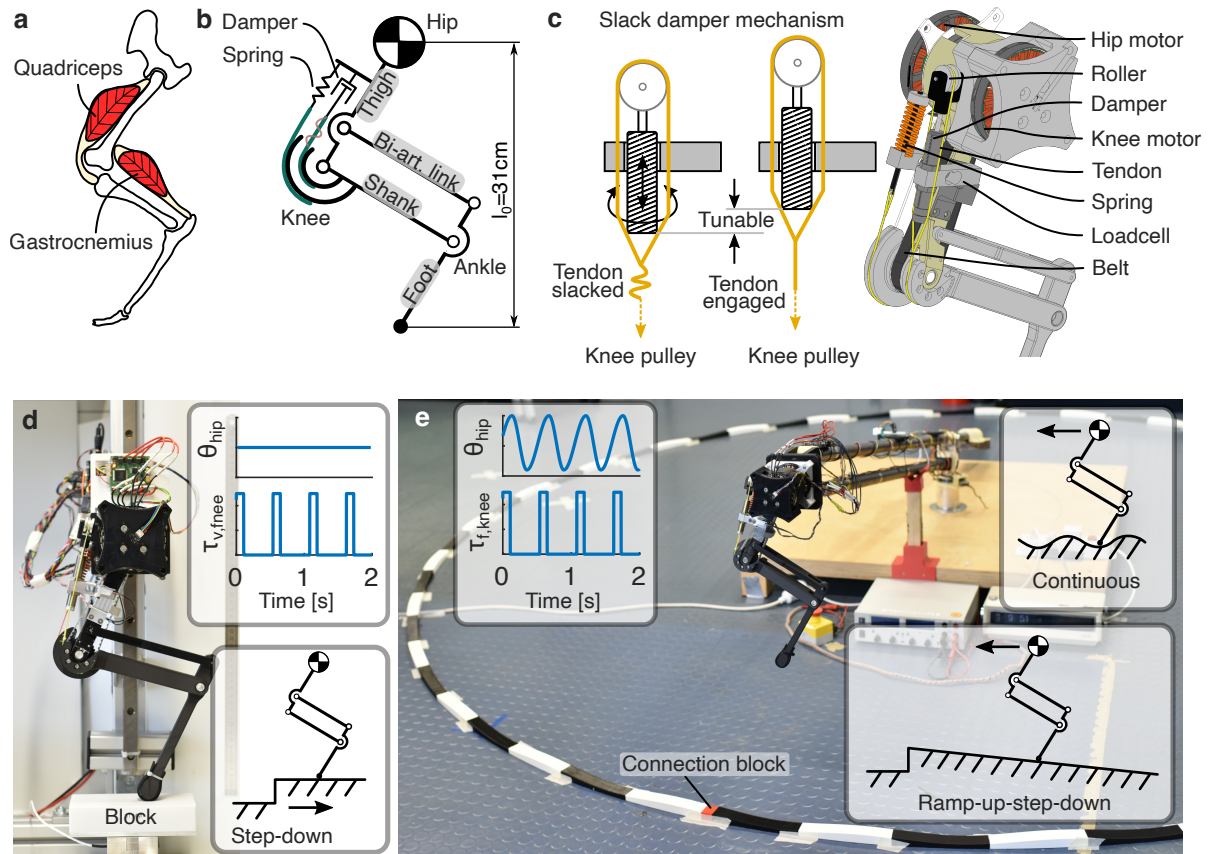


Figure 5. Experiment setup overview. (a) Our leg design is inspired by the leg anatomy of mammalian quadrupeds. (b) We implement a pantograph leg design with spring and damper representing the passive compliance of the quadriceps and a biarticular segment simplifying the gastrocnemius muscle and the Achilles tendon. (c) The rendering of the design shows that the knee joint is coupled to the linear spring, linear damper through tendons, and the knee motor through a timing belt. By rotating the damper with a threaded connection to the loadcell, the damper will travel up and down, thus allowing space for tendon slack. (d) The vertical hopping setup fixes the robot leg on a vertical slider to test step-down perturbation, which is introduced by removing the perturbation block on top of the force sensor. The top right shows a feed-forward control pattern for hip position and knee torque. (e) The forward hopping setup fixes the robot leg on a rotary boom to test continuous perturbation (in photo) and ramp-up-step-down perturbation (Supplementary Movie S3). The top right shows a feed-forward CPG control pattern for hip position and knee torque.

Supplementary Materials for Slack-based tunable damping leads to a trade-off between robustness and efficiency in legged locomotion

An Mo^{1,*}, Fabio Izzì^{1,2}, Emre Cemal Gönen¹, Daniel Haeufle^{2,3}, and Alexander Badri-Spröwitz^{1,4}

¹Dynamic Locomotion Group, Max Planck Institute for Intelligent Systems, Stuttgart, 70569, Germany

²Hertie Institute for Clinical Brain Research and Center for Integrative Neuroscience, University of Tübingen, Tübingen, 72076, Germany

³Institute for Modelling and Simulation of Biomechanical Systems, Computational Biophysics and Biorobotics, University of Stuttgart, Stuttgart, 70569, Germany

⁴Department of Mechanical Engineering, KU Leuven, Leuven, 3001, Belgium

*Corresponding author: An Mo, mo@is.mpg.de

ABSTRACT

The PDF file includes:

Figure S1
Tables S1 to S5
Legends for movies S1 to S3

Other Supplementary Material for this manuscript includes the following:

Movies S1 to S3
Matlab scripts for data analysis: <https://keeper.mpg.de/d/4b9bc3bb7dcb4cbb81c7/>
Computer-aided design of the robot: <https://keeper.mpg.de/d/309550dd51664c01b92b/>

1 Leg design parameters

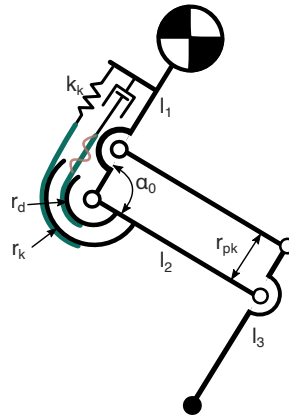


Figure S1. Schematics of the leg with the key design parameters.

Parameters	Value	
Robot mass - vertical hopping	m_v	1.94 kg
Robot mass - forward hopping	m_f	0.94 kg
Leg resting length	l_0	310 mm
Segment 1 length	l_1	150 mm
Segment 2 length	l_2	150 mm
Segment 3 length	l_3	150 mm
Knee spring pulley radius	r_k	30 mm
Knee damper pulley radius	r_d	20 mm
Knee spring stiffness	k_k	10.9 N/mm
Bi-articular insertion radius	r_{pk}	32 mm
Knee resting angle	α_0	100°

Table S1. Robot design parameters.

2 Robot control parameters

Parameters		Value
Vertical hopping		
Hopping frequency	f_v	2.2 Hz
Knee torque amplitude	τ_v	4.0 - 4.3Nm
Knee duty cycle	—	0.22
Forward hopping		
Hip amplitude	θ_{hip}	18°
Hip offset	O_{hip}	2°
Hopping frequency	f_f	1.85 Hz
Hip virtual duty factor	D_{vir}	0.4
Knee torque amplitude	τ_f	1.3 Nm
Knee phase shift	—	0.75
Knee duty cycle	—	0.2

Table S2. Robot control parameters

3 Experimental results

Perturbation [LL]	Damper slack [mm]	Hop height [mm]	CoH [I]	Recovery steps [I]	Delay [ms]	E _d [mJ]
10%	10	53.3	6.3	2.5	-	1
10%	6	49.3	6.6	1.7	51	26
10%	3	49.1	6.7	2.0	26	117
10%	0	44.7	7.4	2.9	0	186
15%	10	55.8	6.3	3.2	-	1
15%	6	47.8	6.7	2.5	50	29
15%	3	43.2	7.0	3.6	24	86
15%	0	42.4	7.6	5.9	0	152

Table S3. Experimental results of vertical hopping with step-down perturbation. The energy dissipated by the damper (E_d) is calculated by integrating the damping force with respect to the damper compression (Fig. 2c).

Roughness amplitude [mm]	Damper slack [mm]	Speed [m/s]	CoT [I]	Step cycle std [ms]
0	10	0.80	1.01	27.1
0	6	0.79	0.99	16.2
0	3	0.71	1.07	2.4
0	0	0.67	1.35	2.1
±5	10	0.76	0.75	2.4
±5	6	0.76	1.01	13.4
±5	3	0.74	1.01	11.1
±5	0	0.68	1.24	2.2
±10	10	0.76	0.79	3.1
±10	6	0.71	0.97	3.6
±10	3	0.72	0.80	2.7
±10	0	0.66	1.32	2.7

Table S4. Experimental results of forward hopping with continuous perturbation.

Perturbation [LL]	Damper slack [mm]	Speed [m/s]	CoT [l]	Recovery steps [l]	Failure steps [l]
15%	10	0.81	0.95	2.7	7
15%	6	0.78	1.00	2.0	4
15%	3	0.72	1.36	1.7	6
15%	0	0.68	1.30	1.0	0
30%	10	0.80	0.91	2.6	10
30%	6	0.75	0.93	2.4	10
30%	3	0.73	1.18	2.9	10
30%	0	0.64	1.44	2.3	3

Table S5. Experimental results of forward hopping with ramp-up-step-down perturbation.

4 Supplementary Videos

Movie-S1: Vertical hopping with step-down perturbation. The leg is hopping on a block whose height is 15% of the leg length. The slack of the damper is set to 3 mm. The first part of the video shows the experiment in real-time. In the second part, slow motion of the same experiment is repeated. In both cases, hip position y , GRF, spring and damper forces are plotted synchronized to the video. In the last part, the phase plots of the all experiments show the relation between hopping speed and the hopping position.

Movie-S2: Forward hopping with continuous perturbation. The leg moves forward by hopping on the sinusoidal terrain with ± 10 mm amplitude. The damper is fully engaged, i.e., the slackness is 0 mm. After the leg completes one full rotation on the terrain, the video shows frames taken by the high-speed video camera.

Movie-S3: Failure modes of forward hopping with ramp-up-step-down perturbation. The leg moves on the flat surface, and it gradually climbs on the ramp to jump off. The perturbation height is 30% of the leg length, and the damper slack is set to 3 mm. The bottom-right plot shows the synchronized hip position in planer motion. The video shows three cases: slipping, stopping, and the good response after the step-down perturbations. The slipping case can be identified by audio irregularity.